IEEE Access
Multidisciplinary | Rapid Review | Open Access Journal

Received August 23, 2021, accepted September 13, 2021, date of publication September 23, 2021, date of current version October 5, 2021.

Digital Object Identifier 10.1109/ACCESS.2021.3115350

A Moving Target Deception Jamming Method Based on Fast Azimuth-Domain Block EM Calculation Against SAR-GMTI

MANG TANG, QINGYANG SUN, TING SHU, (Member, IEEE), KAI-BOR YU, (Life Senior Member, IEEE), WENXIAN YU, (Senior Member, IEEE), AND CHANGQING XU, (Member, IEEE)

Shanghai Key Laboratory of Intelligent Sensing and Recognition, Shanghai Jiao Tong University, Shanghai 200240, China

Corresponding author: Ting Shu (tingshu@sjtu.edu.cn)

ABSTRACT This paper presents a novel moving target deception jamming method against synthetic aperture radar (SAR)-ground moving target indication (GMTI) based on fast azimuth-domain block EM calculation. In this method, a fast electromagnetic(EM) calculation based on equivalent bistatic scattered fields is used to simulate the scattering characteristics of moving false target, which greatly improves the computational efficiency. With the azimuth-domain block implementation, the jammer's frequency response (JFR) can be calculated by fast searching and interpolating with EM database, and the computation load is further reduced. The implementation and the performance of the proposed method are discussed. Comparing with the traditional methods based on a point model, the proposed method is able to generate more verisimilar moving false targets for different attitudes and resolutions. The simulation experiments are provided to demonstrate the validity of the proposed method.

INDEX TERMS Synthetic aperture radar (SAR), deception jamming, moving target, electromagnetic (EM) calculation.

I. INTRODUCTION

Due to capability of all-weather, all-day, and high-resolution imaging, synthetic aperture radar (SAR) has been a powerful technique in both civil and military field [1], [2]. As an important application of SAR, ground moving target indication (GMTI) has played an important role in detection, location and imaging of moving targets [3]. In order to prevent the SAR-GMTI system from acquiring the accurate moving target information, the electronic countermeasure (ECM) against the SAR-GMTI system has attracted many attentions and various jamming methods have been developed [4]. Moreover, the research on jamming methods can help identify the weakness of the SAR-GMTI system and improve it in the future.

In general, jamming methods against the SAR-GMTI system can be classified as barrage noise jamming and deception jamming method. For barrage noise jamming method [5], strong noise-like signals are used to prevent the hostile forces from obtaining information of the moving target while keeping its easy realization. However, the jamming requires a very high jamming power and has the low concealment purpose. In the deception jamming way [6]–[11], it can simulate the characteristics of moving target echoes so that false moving targets can be generated in SAR image. In contrast, the deception jamming technique needs less jamming power, and produces false signals similar to real echoes while haves the same processing gains as real echoes. Thus, the deception jamming method is always a hot topic in the SAR-GMTI ECM.

Meanwhile, the SAR automatic target recognition(ATR) systems can be classified into two groups according to the descriped target characteristics, one is the template-based system and another is the model-based system. For the template-based systems, the targets are described by a large database of templates, which are performed by storing the target's SAR images at different view of angles. However, the performances of ATR degrade sharply when the test samples and template ones are not quite alike because of the lack of corresponding templates. The systems based models utilizes the physical or conceptual models of the targets to describe the target characteristics. The SAR images or feature at various conditions can be predicted, and then be used as the reference for target recognition. In contrast, the model-based one cannot only predict the features of targets at arbitrary

The associate editor coordinating the review of this manuscript and approving it for publication was Su Yan.

attitudes and geometry configurations, but also provide physical descriptions for the targets.

Similarly, the deception jamming techniques against the SAR-GMTI system can be categorized as template-based ones and model-based ones. Most of the existing deception jamming techniques are focused on template-based techniques [15]–[18]. Some of the techniques focus on generating jamming signals for static extended scenes, which can be regarded as static jamming and have limited impact on the SAR-GMTI system. In addition, the moving target deception jamming (MTDJ) methods can generate jamming signals, which can simulate the echo characteristics of the moving target through a single jammer or multiple jammers. They lead to the good performance of the deception jamming against the single-channel or multiple-channel SAR-GMTI system. However, the defect of limited template samples has also not been overcome for the template-based deception jamming techniques. Therefore, this paper focuses on the model-based deception jamming method against the SAR-GMTI system. Contributions include: 1) satisfying the demand of deception jamming for different attitudes and resolutions; 2) good countermeasure performance against model-based recognition methods.

Based on previous works, this paper presents a novel moving target deception jamming method against SAR-GMTI based on fast azimuth-domain block electromagnetic(EM) calculation. First, a fast EM calculation based on equivalent bistatic scattered fields is used to simulate the scattering characteristics of moving false target, which greatly improves the computational efficiency. Then, with the azimuth-domain block implementation, the jammer's frequency response (JFR) can be calculated by fast searching and interpolating with EM database and the computation load is further reduced. Finally, by multiplying between the proposed JFR and the intercepted radar signal spectrum, the deception jamming can be realized in real time. Several simulation results are performed to validate the proposed method.

The rest of this paper is organized as follows. The signal models are introduced in Section II. The deception jamming method based on fast azimuth-domain block EM calculation are proposed in Section III. The performance of the algorithm is discussed in Section IV. Section V shows the simulation results. Section VI concludes this paper.

II. SIGNAL MODELS

A. GEOMETRY CONFIGURATION

Fig.1 shows the geometry configuration for deceptive jamming against the SAR-GMTI system. It is assumed that the SAR platform flies with a constant velocity V along y direction. The initial position of SAR is $(0, 0, H)$ in the Cartesian coordinate system $Oxyz$ at azimuth time $\eta = 0$. The jammer is located at $(x_J, 0, z_J)$ in $Oxyz$. The centroid of a moving target is placed at $(x_t, y_t, 0)$ with a constant range and azimuth velocity v_x and v_y, respectively.

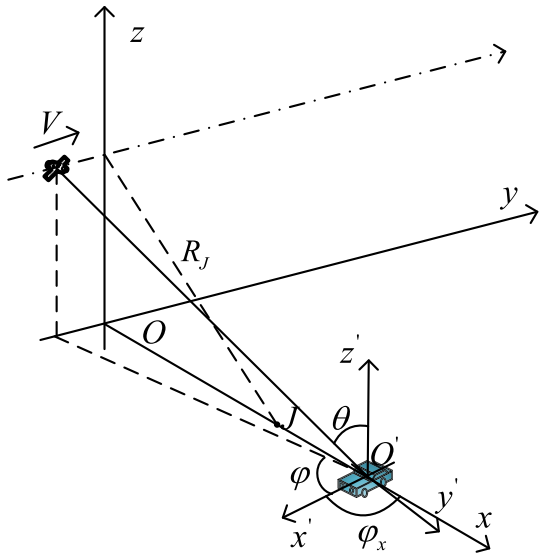

FIGURE 1. The geometry configuration for deceptive jamming against SAR.

According to Fig.1, the instantaneous slant range from the radar to the jammer is given by

$$R_J(\eta) = \sqrt{x_J^2 + V^2\eta^2 + (H - z_J)^2} \tag{1}$$

The instantaneous slant range from the radar to the centroid of the moving target is expressed as

$$R(\eta) = \sqrt{(x_t + v_x\eta)^2 + (y_t + v_y\eta - V\eta)^2 + H^2} \tag{2}$$

Let $\Delta R(\eta) = R(\eta) - R_J(\eta)$, and $\Delta R(\eta)$ determines the range and Doppler modulation of the false target during the deception jamming.

Meanwhile, we define another coordinate system $O'x'y'z'$ in order to describe the instantaneous relation between the moving target and the SAR-GMTI system [9]. The origin O' locates at the centroid of the moving target, which moves with the false target. The x'-axis is the horizontal axis of symmetry of the target, the z'-axis is upward positive, and the y'-axis is determined by the right hand rule, as shown in Fig.1.

Because the synthetic aperture time is relatively short, the typical movement of a moving target can be regarded as a linear motion at a uniform speed or acceleration, thereby ignoring the changes in the look angle caused by rotation. Meanwhile, the rigid non-rotational motion of the target does not change the inclination and azimuth information of the moving target under the far-field approximation. Suppose the instantaneous inclination angle and azimuth angle of the moving target relative to the SAR-GMTI system are denoted by θ and φ respectively. Therefore, they are expressed as

$$\theta = \arccos\left(\frac{H - z_0}{R_0}\right) \tag{3}$$

$$\varphi = \pi - \arctan\left(\frac{-V\eta}{x_0}\right) - \varphi_0 \tag{4}$$

where φ_0 is initial azimuth angle of the target at the azimuth time $\eta = 0$, and x_0 is initial position of the target in the x-axis. θ and φ determine the EM model modulation of the false target during the deception jamming. They describe the attitudes of the false target and determine which part of the electromagnetic model of the false target is selected.

B. DECEPTION JAMMING MODEL

Suppose the SAR transmits linear frequency modulation (LFM) signal. Hence, the baseband echoes intercepted by the jammer can be expressed as

$$s_J(\tau,\eta) = \omega_r(\tau - \frac{2R_J(\eta)}{c}) \times \exp(-j2\pi f_c \frac{2R_J(\eta)}{c}) \times \exp(-j\pi K_r(\tau - \frac{2R_J(\eta)}{c})^2) \quad (5)$$

where τ is the range time, $\omega_r(\tau)$ is a rectangular window with center 0 and pulse width T_r, f_c is the carrier frequency, and K_r is the chirp rate. $R_J(\eta)$ is the range to the jammer from the SAR, and c is the speed of the light.

If the deceptive target existed, its echo can be given by

$$s(\tau,\eta) = \int\int\int \sigma(x,y,z)dxdydz \times\omega_r(\tau - \frac{2R_t(\eta)}{c}) \exp(-j2\pi f_c \frac{2R_t(\eta)}{c}) \times \exp(j\pi K_r(\tau - \frac{2R_t(\eta)}{c})^2) \quad (6)$$

where $\sigma(x,y,z)$ is the backscattering coefficient of a point scatterer in the deceptive target, which is located at (x,y,z) in the target deception coordinates system. $R_t(\eta)$ is the instantaneous slant range from the radar to each scatterer of the moving target.

To achieve the deceptive jamming, the jammer intercepts the signals emitted by the radar, denoted by $s_J(\tau,\eta)$, and then performs a modulation of the amplitude, time delay and Doppler on the intercepted radar signal in order to generate the echoes of false targets, denoted by $s(\tau,\eta)$. In practical application, the modulation of the time delay is achieved in frequency domain to acquire a quick realization.

Then, the jammer's frequency response(JFR) can be expressed as

$$H(f_\tau,\eta) = \int\int\int \sigma(x,y,z)dxdydz \times \exp(-j\frac{4\pi(f_c+f_\tau)}{c}\Delta R_t(\eta)) \quad (7)$$

where f_τ is the range frequency, and $\Delta R_t(\eta) = R_t(\eta) - R_J(\eta)$ is the range difference.

As for the JFR, $\sigma(x,y,z)$ describes the scattering characteristics of the false target, which determines whether the false target is similar to the real one or not. In the template-based deception jamming methods, $\sigma(x,y,z)$ is denoted by the deception-templates, which are usually derived from an existing SAR image. However, the false target generated by these methods is difficult to be able to include the similar structural or scattering information relative to the SAR-GMTI system. Therefore, in the model-based deception jamming method, the EM model is used to denote the scattering characteristics of the false target, as expressed by $\sigma(x,y,z)$.

III. THE PROPOSED METHOD

A. FAST EM CALCULATION

Because the range from the SAR to the deceptive target is usually much larger than the size of the target, $R_t(t_a)$ can be approximately equal to the summation of the range from the origin to the radar, denoted by $R_o(t_a)$, and the projection of the vector from the origin to the point on the vector of directed from the radar to the origin [11]. It can be denoted by [19]

$$R_t(\eta) \approx R(\eta) + |\vec{r}|\frac{\vec{r}\times\vec{k_i}}{|\vec{r}|\left|\vec{k_i}\right|} \quad (8)$$

$$\vec{r} = x\vec{x} + y\vec{y} + z\vec{z} \quad (9)$$

$$\vec{k_i} = -\left[\sin\varphi\cos\theta\vec{x} + \sin\varphi\sin\theta\vec{y} + \cos\varphi\vec{z}\right] \quad (10)$$

where $|\cdot|$ is the length of the vector, $\vec{r} = \vec{OT}$, and $\vec{k_i}$ is the unit vector of $\vec{SO}$.

Substituting (9) and (10) into (8), one obtains

$$R_t(\eta) = R(\eta) - \left[\sin\varphi\cos\theta x + \sin\varphi\sin\theta y + \cos\varphi z\right] \quad (11)$$

Substituting (11) into (7), one obtains

$$H(f_\tau,\eta) = \exp\left[-j\frac{4\pi(f_\tau+f_c)}{c}\Delta R(\eta)\right] \times E(\theta,\phi,f_\tau) \quad (12)$$

with

$$E(\theta,\varphi,f_\tau) = \int\int\int \sigma(x,y,z)\exp(-j2k\vec{k_i}\times\vec{r})dxdydz \quad (13)$$

where $E(\theta,\varphi,f_\tau)$ is the frequency response of electromagnetic scattering from the deceptive target [20], and $H(f_\tau,\eta)$ in (12) is the proposed JFR.

It is evident that the motion modulation of false target is determined by the first exponential term of Equ.(12), including the range delay modulation and azimuth Doppler modulation. In addition, the EM scattering modulation of false target is determined by the last term of Equ.(12), since it can be approximated as the backscattered fields at the far field for different look angles [20].

To calculate the scattered fields from complex target, the SBR technique combining geometrical optics (GO) and physical optics (PO) is utilized in this paper to efficiently calculate the first-bounce physical optics, the physical theory of diffraction contributions, and the multi-bounce contributions [21], [22]. For simplicity, we utilize an EM calculation tool, like CST Microwave Studio [23] to obtain the results of SBR method. According to the computational complexity, the SBR algorithm can be divided into two parts, one is ray tracing and another is associated EM calculation [22]. Generally, if you consider a detailed object model, the former part not only consumes most of the computing resources, but also needs to be performed for each observation angle when calculating the monostatic scattered fields. By constrast, it is more efficient

to obtain the bistatic scattered field data because ray tracing is performed only once for the incident direction and only the EM calculation are required for each viewing angle [11].

Thus, we utilize the monostatic bistatic equivalence principle to greatly accelarate the calculation of EM scattering [24]. The relationship is given by

$$\sigma(\theta = \frac{\Theta}{2}, f) = \sigma_b(\theta = \Theta, f\cos(\frac{\Theta}{2})) \tag{14}$$

where σ and σ_b is the monostatic and bistatic radar cross section (RCS), recpectively, f is the carrier frequency, θ is the receiver look angle, and Θ is the bistatic angle. This means that the bistatic RCS equals the monostatic RCS observed at the bisecting angle for a different carrier frequency f. The frequency change is indicated in Equ.(14) by the factor $\cos(\Theta/2)$. Therefore, this effect can be regarded as a corresponding change in wavelength. From this perspective, it is obvious that the small bistatic angle has little effect on the wavelength, while the effect on RCS is negligible in many aspects. Therefore, we utilize the EM calculation based on equivalent bistatic scattered fields computed from the SBR technique to simulate the scattering characteristics of the false target, which greatly improves the computational efficiency.

B. AZIMUTH-DOMAIN BLOCK

Although the fast EM calculation is utilized to calculate the EM scattering complex large targets, the amount of calculation required is still large especially while satisfying the needs of deception jamming for the false targets in all attitudes. Therefore, in order to further reduce the computational burden, this paper introduces the idea of azimuth block. In this method, the point-by-point update is changed to the block-by-block update, and the block can still be quickly realized by the equivalent bistatic scattered field. In addition, it is beneficial to use parallel processing for the blocking strategy, and then to quickly search the required target RCS data from the EM database after the segmentation. It further reduces the amount of real-time calculation.

When performing the deception jamming, the scattering characteristics of the false target over the synthetic azimuth angle is usually interested. Therefore, we divide the azimuth angle from 0 to 360 degrees into multiple blocks with the synthetic azimuth angle θ_{bw} as the step size. Then the number of azimuth blocks existing in the electromagnetic model database can be expressed as

$$N = ceil(\frac{360}{\theta_{bw}}) \tag{15}$$

where $ceil(\cdot)$ returns the value of a number rounded upwards to the nearest integer, $\theta_{bw} = 0.886\lambda/L_a$, λ is the wavelength, and L_a is the antenna length along the azimuth direction [1].

Then, the azimuth angle of the kth block for the monostatic scattered data ranges from $k \cdot \theta_{bw} - \frac{1}{2}\theta_{bw}$ to $k \cdot \theta_{bw} + \frac{1}{2}\theta_{bw}$, where $k = 1, 2, \ldots, N$, and $k \cdot \theta_{bw}$ is the center incidence angle of the kth block. According to the equivalence theorem, the azimuth angle of the kth block for the equivalent bistatic scattered data ranges from $k \cdot \theta_{bw} - \theta_{bw}$ to $k \cdot \theta_{bw} + \theta_{bw}$, where $k \cdot \theta_{bw}$ is still the incidence angle of the kth block. Considering that the bistatic angle in each block is consistent with the synthetic azimuth angle, the frequency shift term in the equivalence can be ignored because the bistatic angle in the simulation is very small, as expressed by Equ.(14). For a typical SAR system, there are thousands of different viewing angles within the length of the synthetic aperture. Although the RCS of false targets at these observation angles can calculated by using equivalent bistatic scattering fields, it is still very computationally time-consuming.

Therefore, this paper consider a strategy, which is downsampling in azimuth first. The azimuth sampling interval after downsampling is $\Delta\theta$. The larger $\Delta\theta$, the smaller the amount of calculation required. However, if the sampling interval is too large, it leads to a large azimuth angle error and appearing ghost targets in azimuth pairs, which can severely affect the performance of deception jamming. Section IV will focus on the analysis of the azimuth modeling.

While we perform the deception jamming against the SAR-GMTI system and want to generate a false target at a certain attitude θ_0, the corresponding azimuth block should be found at first. The index of the block can be calculated as

$$M = ceil(\frac{\theta_0}{\theta_{bw}}) \tag{16}$$

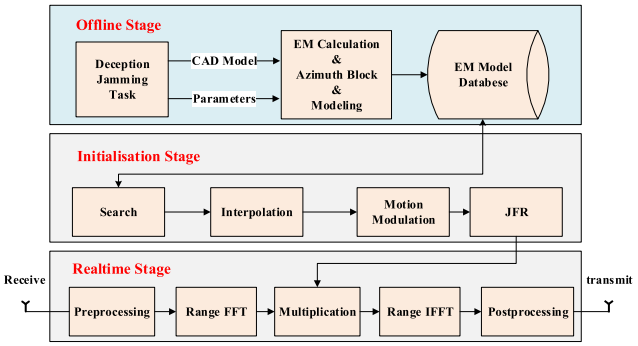

FIGURE 2. Block diagram of MTDJ against multichannel SAR-GMTI.

Then, the block's scattered data is up-sampled by interpolation along the azimuth to obtain the RCS data of the false target at all the observation angles of SAR of the synthetic azimuth angle.

C. IMPLEMENTATION SCHEME

To sum up, the block diagram of the proposed algorithm is shown in Fig.2. The process of a deceptive jammer is separated into three stages: the offline calculation stage, the initialisation stage and the realtime modulation stage.

1) OFFLINE CALCATION STAGE

This stage is to build the EM scattering database. According to the deception jamming task, the EM database is established offline from the target CAD model utilizing the fast EM calculation method. The CAD model with user-defined

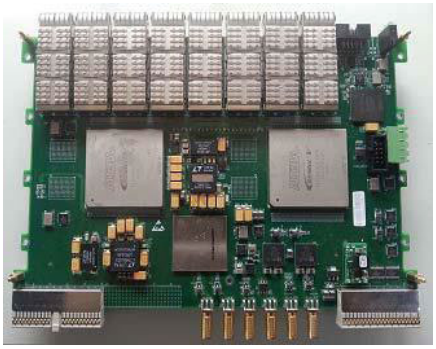

FIGURE 3. The wideband DRFM board.

mechanical material behavior has the electromagnetic property. This stage is defined as the offline calculation stage.

2) INITIALISATION STAGE

The initialisation stage is to obtain the JFR. The JFR is computed according to Equ.(12), including the EM scattering modulation and the motion modulation. In practical application, we use the local DDR SDRAM of digital radio frequency memory (DRFM) board to store the JFR.

For practical consideration, a typical wideband DRFM board with 1GHz bandwidth is shown in Fig.3, which plays the role of real-time SAR signal acquisition and wideband jamming signal generation. The board shown in Fig.3 contains two large scale field programmable gate arrays (FPGA), one 12-bit high-speed ADC sampling at 2.8GHz, and two 12-bit high-speed DAC sampling at 2.8GHz. Two independent DDR SDRAM banks are configured with each of DRFM board. In order to store the JFR, each DDR SDRAM banks is designed up to 1GB deep. This memory deep is sufficient for most SAR jamming.

3) REALTIME MODULATION STAGE

The last stage is called the real-time modulation stage. In practical application, the deception jamming is realized in real time by multiplying between the proposed JFR and the intercepted radar signal spectrum. In addition, it usually contains a series of preprocessing, range fast fourier transform (FFT), range inverse FFT (IFFT) and a series of postprocessing within the FPGAs of wideband DRFM board.

IV. PERFORMANCE ANALYSIS

As mentioned above, the electromagnetic model of the target is represented by a discrete data sequence and changes with the frequency and attitude angle [9]. In general, it is impossible to simulate the EM scattering of the target in every tiny pose and range frequencies because it is limited by the calculation complexity and the size of database. Hence, the model of the EM database affects the performance of the deception jamming. The following part will analyze the factors affecting the performance of the proposed algorithm.

A. AZIMUTH MODELING OF THE EM DATABASE

Assuming that the synthetic azimuth angle of the SAR-GMTI systems is β_{bw}, the corresponding azimuth angle for the i-th block ranges from $-\frac{\beta_{bw}}{2}+\beta_i$ to $\frac{\beta_{bw}}{2}+\beta_i$, where $\beta_i = i\cdot\beta_{bw}$ is the center azimuth angle of the i-th block. Then, the azimuth resolution of the SAR-GMTI system is

$$\Delta_y = \frac{\lambda}{2\beta_{bw}} \tag{17}$$

Suppose the biggest size of the target in azimuth is L_y, then the count of points in the azimuth dimension is

$$N_y = \frac{L_y}{\Delta_y} \tag{18}$$

The azimuth angle interval should be less than

$$\Delta\phi = \frac{\beta_{bw}}{N_y} = \frac{\lambda}{2L_y} \tag{19}$$

where $\Delta\phi$ is related not to the azimuth synthetic angle of the SAR-GMTI system but to the maximum size of a target in azimuth.

When the azimuth interval is greater than $\Delta\phi$, the biggest size of a target in the azimuth of SAR imaging results, denoted by L_y, is decreased. It leads to the azimuth aliasing of the target, i.e. the ghost target, and the reduction of the effectiveness of deception jamming as well.

B. FREQUENCY MODELING OF THE EM DATABASE

The stepped frequency waveform (SFW) is utilized to simulate the frequency response of the scattering. Assuming that the bandwidth of the SAR-GMTI systems is B_w, the corresponding frequency for each block ranges from $-\frac{B_w}{2}$ to $\frac{B_w}{2}$. Then, the range resolution of the SAR-GMTI system is

$$\Delta_x = \frac{c}{2B_w} \tag{20}$$

Suppose the biggest size of a target in range is denoted L_x, then the count of points in the range dimension is

$$N_x = \frac{L_x}{\Delta_x} \tag{21}$$

Similarly, the range frequency interval should be less than

$$\Delta f = \frac{B_w}{N_x} = \frac{c}{2L_x} \tag{22}$$

where Δf is related to the maximum size of a target in range.

C. ELEVATION MODELING OF THE EM DATABASE

Assuming that the elevation ranges from θ_{max} to θ_{min}. Then, the elevation resolution of the SAR-GMTI system is

$$\Delta_z = \frac{\lambda}{2\theta_{bw}} \tag{23}$$

where $\theta_{bw} = \theta_{max} - \theta_{min}$.

Suppose the biggest size of a target in elevation is denoted L_z, then the count of points in the elevation dimension is

$$N_z = \frac{L_z}{\Delta_z} \tag{24}$$

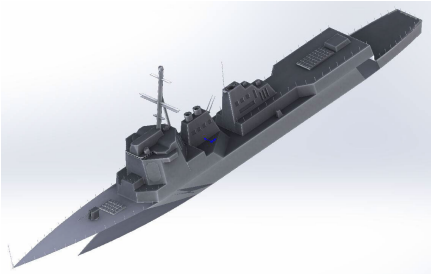

FIGURE 4. The CAD model of a destroyer.

Similarly, the elevation angle interval should be less than

$$\Delta\theta = \frac{\theta_{bw}}{N_z} = \frac{\lambda}{2L_z} \tag{25}$$

where $\Delta\theta$ is related to the biggest size of a target in elevation.

V. SIMULATION

A. STATISTICAL CHARACTERISTICS

In this simulation, multiple simulated images of a target, i.e., a simple destroyer, are added to analyze the deception jamming performance. Fig. 4 is the high precision 3-D CAD model of the destroyer, whose length and width are roughly equivalent to 161.8 m and 20 m, respectively. On one hand, we generate the simulated SAR images by using the simulated data, which are calculated by the EM code. In the simulation, the frequency ranges from 2.925 to 3.075 GHz with a step of 0.75MHz, and the azimuth angles ranges from $\phi - \frac{\beta_{bw}}{2}$ to $\phi + \frac{\beta_{bw}}{2}$ with an interval of 0.01435°. β_{bw} is the synthetic aperture, and ϕ is the incident center azimuth angle. On the other hand, we generate the deceptive SAR images by using the deception jamming signals, which are generated by the proposed method. Based on the above analysis, the frequency is still stepped from 2.925 to 3.075 GHz to guarantee proper unambiguous range. As for the bistatic case, the incident azimuth angle is at ϕ and the scattered fields are observed from $\phi - \beta_{bw}$ to $\phi + \beta_{bw}$ with an interval of 0.0287°.

Fig.5 shows the simulated SAR images and the deceptive SAR images at 40° and 85° center azimuths at 45° elevation. It can be seen that the deceptive target and the simulated SAR target have similar image intensities, which indicates the effectiveness of the proposed method. In general, geometric features are widely used in SAR ATR system. In order to avoid the interference of sea clutter, the extraction can be carried out in the minimum boundary rectangle around the target. Table 1 compares the geometrical characteristic of target in the simulated images with those in the deceptive images, including the length and width. As shown in Table 1, the errors of the geometrical features between the simulated and deceptive targets are small. On the other hand, the structure similarity (SSIM) is introduced to quantitatively evaluate the similarity between the deceptive targets and the simulated ones [6]. It varies between 0 and 1, and the larger the value is, the better the performance of the jamming method will be. The SSIM of each image is also listed, where the higher the value, the better the interference performance. Simulation results show that this method can generate deceptive targets with different attitudes in high fidelity.

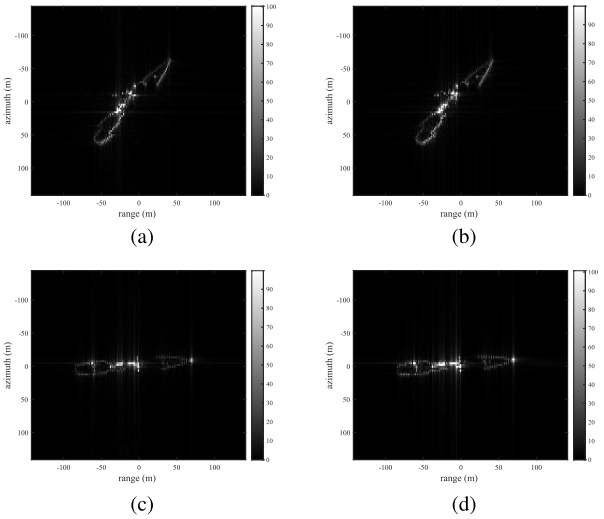

FIGURE 5. The comparison between simulated SAR images and deceptive SAR images. (a) simulated SAR image at 40°. (b) deceptive SAR image at 40°. (c) simulated SAR image at 85°. (d) deceptive SAR image at 85°.

TABLE 1. The feature evaluation between the simulated target and the false target.

ID	Angle(°)	Length(m)	Width(m)	SSIM
40°simulated target	40.1	160.19	19.98	94.5%
40°deceptive target	40.2	159.32	19.99	
85°simulated target	85.1	158.22	19.81	93.7%
85°deceptive target	84.7	157.89	19.80	

B. DECEPTION JAMMING RESULTS

In this section, general deceptive jamming simulation experiments are carried out on static scenes and moving objects to verify the proposed simulation method. Table 2 shows the simulation system parameters. In this experiment, we aim to plant moving deceptive targets into the real scene. The actual SAR image obtained by the spaceborne SAR system is shown in the Fig. 6, which is used as a reflectivity map of the false static scene before the deceptive jamming. The scene size is 1024 × 024 pixels, and the sampling intervals in the azimuth and range directions are 3m and 1m, respectively. In addition, three false targets were embedded in the selected

TABLE 2. The simulation parameters.

Parameter	Value	Unit
Carrier Frequency	3.0	GHz
Chirp Bandwidth	150	MHz
Sampling Frequency	165	MHz
Pulse Repetition Frequency	4147.2	Hz
Platform Velocity	7113.59	m/s

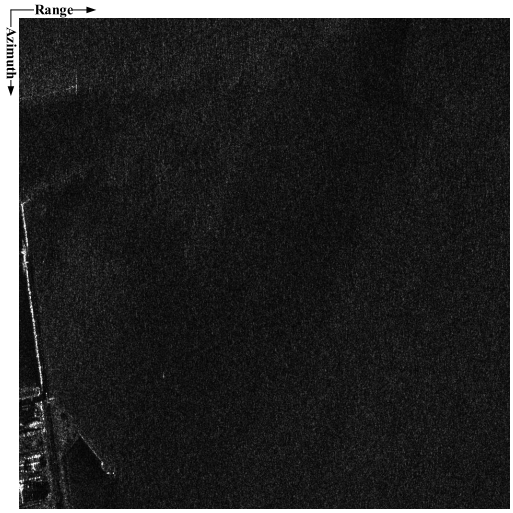

FIGURE 6. The real scene.

patch. The three targets are numbered T1 to T3, and their motion parameters are shown in Table 3.

TABLE 3. The motion parameters.

Target	range	azimuth	range velocity
T1	-250m	-150m	- 3.5m/s
T2	0m	50m	3.5m/s
T3	250m	400m	10m/s

In order to better describe the performance of the proposed method, we perform comparative experiments on static deceptive targets with zero motion parameters. According to the proposed method, we first generate the deception jamming signals for the three false targets. The imaging result of the interference signal is then obtained by using ωK imaging algorithm [1]. Fig. 7 shows the imaging results after the deceptive jamming. It is seen that the moving deceptive targets ($T1$ to $T3$) with range velocity in Fig. 7b shows the azimuth shift effect comparing with the static deceptive targets in Fig.7a.

TABLE 4. The measured azimuth shift values.

Target	Azimuth Shift		
	Theory	Proposed Method	Error
$T1$	-273.4m	-272.7m	0.3%
$T2$	273.6m	274.4m	0.3%
$T3$	782.1m	782.1m	0.0%

In general, the azimuth shifts can be used as a criterion to evaluate the false echo of a range-velocity moving target [25], [26]. If the target has the velocity v_r in the range direction, its azimuth shifts will be $\Delta x = R_0 \frac{v_r}{v}$. Thus, the measured azimuth shifts is utilized to quantitatively validate the jamming results of the proposed method. Table 4 shows the comparison of the azimuth shifts between the expected theoretical value and the measured ones of the proposed

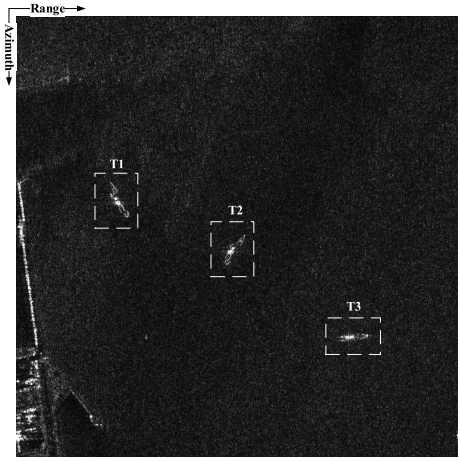

(a)

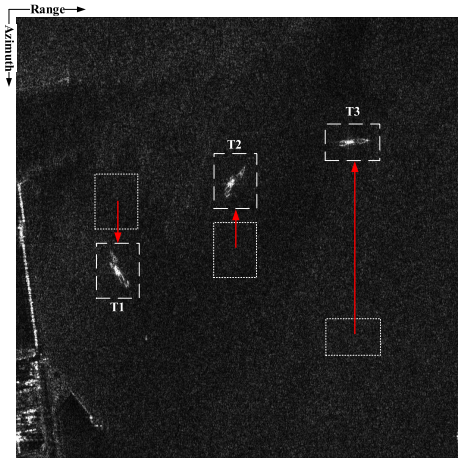

(b)

FIGURE 7. The deception jamming result. (a)static deceptive targets. (b)moving deceptive targets.

FIGURE 8. The deception jamming result of moving false targets with a large azimuth velocity.

method. The results show that the measured values are in good agreement with the theoretical values.

In Fig. 7, static deceptive targets and moving deceptive targets seems like only have different azimuth position because

it only has the range velocity. And if the moving target has a large velocity in the azimuth direction, the moving deceptive target will also become blurred in the azimuth direction[R1], as shown in Fig.R1. The azimuth velocity of the three targets are 100m/s, 45m/s, and 125m/s respectively. Thus, it is demonstrated that this method can generate deceptive targets with high fidelity.

VI. CONCLUSION

In this paper, a novel deceptive jamming method based on fast azimuth-domain block EM calculation for interfering the SAR-GMTI system has been proposed. To generate a verisimilar moving targets, a fast EM calculation based on equivalent bistatic scattered fields is used to simulate the scattering characteristics. It greatly improves the computational efficiency. Then, with the azimuth-domain block implementation, the jammer's frequency response (JFR) can be calculated by fast searching and interpolating with EM database and the computation load is further reduced. Finally, the deception jamming is achieved in real time by a multiplication between the proposed JFR and the spectrum of intercepted radar signals. Simulation results show that the proposed method is very effective to generate the false moving targets with high fidelity against the SAR-GMTI system.

REFERENCES

[1] I. G. Cumming and F. H. Wong, *Digital Signal Processing of Synthetic Aperture Radar Data: Algorithms and Implementation*. Boston, MA, USA: Artech House, 2005.
[2] J. Chen, B. Zhang, and C. Wang, "Backscattering feature analysis and recognition of civilian aircraft in TerraSAR-X images," *IEEE Geosci. Remote Sens. Lett.*, vol. 12, no. 4, pp. 796–800, Apr. 2015.
[3] D. Cerutti-Maori, I. Sikaneta, and C. H. Gierull, "Optimum SAR/GMTI processing and its application to the radar satellite RADARSAT-2 for traffic monitoring," *IEEE Trans. Geosci. Remote Sens.*, vol. 50, no. 10, pp. 3868–3881, Oct. 2012.
[4] W. W. Goj, *Synthetic Aperture Radar and Electronic Warfare*. Norwood, MA, USA: Artech House, 1989.
[5] K. Dumper, P. S. Cooper, A. F. Wons, C. J. Condley, and P. Tully, "Space-borne synthetic aperture radar and noise jamming," in *Proc. IET Int. Radar Syst.*, Oct. 1997, pp. 411–414.
[6] F. Zhou, B. Zhao, M. Tao, X. Bai, B. Chen, and G. Sun, "A large scene deceptive jamming method for space-borne SAR," *IEEE Trans. Geosci. Remote Sens.*, vol. 51, no. 8, pp. 4486–4495, Aug. 2013.
[7] Y. Liu, W. Wang, X. Pan, D. Dai, and D. Feng, "A frequency-domain three-stage algorithm for active deception jamming against synthetic aperture radar," *IET Radar, Sonar Navigat.*, vol. 8, no. 6, pp. 639–646, Jul. 2014.
[8] Q. Sun, T. Shu, S. Zhou, B. Tang, and W. Yu, "A novel jamming signal generation method for deceptive SAR jammer," in *Proc. IEEE Radar Conf.*, May 2014, pp. 1174–1178.
[9] Z. Bo, F. Zhou, X. Shi, Q. Wu, and B. Zheng, "Multiple targets deception jamming against ISAR using electromagnetic properties," *IEEE Sensors J.*, vol. 15, no. 4, pp. 2031–2038, Apr. 2015.
[10] Y. Liu, W. Wang, X. Pan, Q. Fu, and G. Wang, "Inverse omega-K algorithm for the electromagnetic deception of synthetic aperture radar," *IEEE J. Sel. Topics Appl. Earth Observ. Remote Sens.*, vol. 9, no. 7, pp. 3037–3049, Jul. 2016.
[11] Q. Sun, T. Shu, K. Yu, and W. Yu, "Fast target deception jamming method against spaceborne synthetic aperture radar based on equivalent bistatic scattered fields," *J. Eng.*, vol. 2019, no. 21, pp. 7385–7389, Nov. 2019.
[12] Z. Jianxiong, S. Zhiguang, C. Xiao, and F. Qiang, "Automatic target recognition of SAR images based on global scattering center model," *IEEE Trans. Geosci. Remote Sens.*, vol. 49, no. 10, pp. 3713–3729, Oct. 2011.
[13] B. Ding and G. Wen, "A region matching approach based on 3-D scattering center model with application to SAR target recognition," *IEEE Sensors J.*, vol. 18, no. 11, pp. 4623–4632, Jun. 2018.
[14] B. Ding and G. Wen, "Target reconstruction based on 3-D scattering center model for robust SAR ATR," *IEEE Trans. Geosci. Remote Sens.*, vol. 56, no. 7, pp. 3772–3785, Jul. 2018.
[15] L. Huang, C. Dong, Z. Shen, and G. Zhao, "The influence of rebound jamming on SAR GMTI," *IEEE Geosci. Remote Sens. Lett.*, vol. 12, no. 2, pp. 399–403, Feb. 2015.
[16] Q. Sun, T. Shu, K.-B. Yu, and W. Yu, "Efficient deceptive jamming method of static and moving targets against SAR," *IEEE Sensors J.*, vol. 18, no. 9, pp. 3610–3618, May 2018.
[17] Q. Sun, T. Shu, K.-B. Yu, and W. Yu, "A novel deceptive jamming method against two-channel SAR-GMTI based on two jammers," *IEEE Sensors J.*, vol. 19, no. 14, pp. 5600–5610, Jul. 2019.
[18] Q. Sun, T. Shu, M. Tang, K.-B. Yu, and W. Yu, "Effective moving target deception jamming against multichannel SAR-GMTI based on multiple jammers," *IEEE Geosci. Remote Sens. Lett.*, vol. 17, no. 3, pp. 441–445, Mar. 2020.
[19] W. Lv, J. Wang, and W. Yu, "Simulation of echoes from ballistic targets," *IEEE Antennas Wireless Propag. Lett.*, vol. 13, pp. 1361–1364, 2014.
[20] C. Ozdemir, *Inverse Synthetic Aperture Radar Imaging With MATLAB Algorithms*. Hoboken, NJ, USA: Wiley, 2011.
[21] H. Ling, R.-C. Chou, and S.-S. Lee, "Shooting and bouncing rays: Calculating the RCS of an arbitrarily shaped cavity," *IEEE Trans. Antennas Propag.*, vol. 37, no. 2, pp. 194–205, Feb. 1989.
[22] L. John, "XPATCH: A high-frequency electromagnetic-scattering prediction code and environment for complex three-dimensional objects," *IEEE Antennas Propag. Mag.*, vol. 36, no. 1, pp. 65–69, Feb. 1994.
[23] *CST Suite 2013*, CST AG, Darmstadt, Germany, 2013.
[24] R. E. Kell, "On the derivation of bistatic RCS from monostatic measurements," *Proc. IEEE*, vol. 53, no. 8, pp. 983–988, Aug. 1965.
[25] P. R. Kersten, R. W. Jansen, K. Luc, and T. L. Ainsworth, "Motion analysis in SAR images of unfocused objects using time-frequency methods," *IEEE Geosci. Remote Sens. Lett.*, vol. 4, no. 4, pp. 527–531, Oct. 2007.
[26] O. Dogan and M. Kartal, "Efficient strip-mode SAR raw-data simulation of fixed and moving targets," *IEEE Geosci. Remote Sens. Lett.*, vol. 8, no. 5, pp. 884–888, Sep. 2011.

MANG TANG received the B.S. degree in electrical information engineering from Chengdu University of Technology, Sichuan, China, in 1999, and the M.S. degree in information and communication engineering from Southeast University, Nanjing, China, in 2011. He is currently pursuing the Ph.D. degree with Shanghai Key Laboratory of Intelligent Sensing and Recognition, Shanghai Jiao Tong University, Shanghai, China. Since 2006, he has been with Nanjing Research Institute of Electronics Equipment, working on system design and signal processing technique in electronic and information system. His research interest includes radar ECM technique.

QINGYANG SUN received the B.S. degree in electrical information engineering from Northeastern University (NEU), Shenyang, China, in 2012. He is currently pursuing the Ph.D. degree with Shanghai Key Laboratory of Intelligent Sensing and Recognition, Shanghai Jiao Tong University, Shanghai, China. His research interests include radar system modeling and simulation and SAR ECCM and ECM technique.

TING SHU (Member, IEEE) received the B.S. and M.S. degrees in electrical engineering from Nanjing University of Science and Technology, Nanjing, China, in 2004 and 2006, respectively, and the Ph.D. degree in electrical engineering from Shanghai Jiao Tong University (SJTU), Shanghai, China, in 2010. From 2010 to 2011, he was a System Engineer with the Wireless Department, Huawei Technologies Company Ltd., responsible for the baseband system design for the 3G/4G evolution. In 2011, he joined SJTU, where he is currently an Associate Professor with Shanghai Key Laboratory of Intelligent Sensing and Recognition, School of Electronic Information and Electrical Engineering. His current research interests include advanced technology of radar electronic protection (EP), research and development of the hardware-in-loop simulation for radar and EW systems, real-time signal processing technique, and adaptive array for phased array radars.

KAI-BOR YU (Life Senior Member, IEEE) received the B.S. degree in electrical engineering and applied mathematics from Yale University, in 1977, the M.S. degree in electrical engineering from Brown University, in 1979, and the Ph.D. degree in electrical engineering from Purdue University, in 1982. He was an Assistant Professor with the Department of Electrical Engineering, Virginia Polytechnic Institute and State University, from 1982 to 1988. From 1988 to 2001, he was with GE Research and Development Center, Niskayuna, NY, USA, as a Senior Principal Engineer. From 2001 to 2005, he was with Raytheon Company, as a Senior Principal Systems Engineer. From 2005 to 2010, he was with Lockheed Martin Company, as a Principal Systems Engineer. From 2010 to 2013, he was with Boeing Company, as a Principal Systems Engineer. Since September 2015, he has been with Shanghai Jiao Tong University, as a Distinguished Professor. His activities encompassed various topics of phased array radar system design, radar system modeling and simulation, radar ECCM and ECM technique, radar DBF, and super-resolution technique. He holds over 30 U.S. patents in his areas, and has published two book chapters and numerous journal and conference proceeding papers.

WENXIAN YU (Senior Member, IEEE) received the B.S., M.S., and Ph.D. degrees from the National University of Defense Technology, Changsha, China, in 1985, 1988, and 1993, respectively. From 1996 to 2008, he was a Professor with the College of Electronic Science and Engineering, National University of Defense Technology, where he was also the Deputy Head of the College and the Assistant Director of the National Key Laboratory of Automatic Target Recognition. From 2009 to 2011, he was the Executive Dean of the School of Electronic, Information, and Electrical Engineering, Shanghai Jiao Tong University, Shanghai, China, where he is currently a Yangtze River Scholar Distinguished Professor and the Head of the research part with the School of Electronic, Information, and Electrical Engineering. His research interests include remote sensing information processing, automatic target recognition, and multisensor data fusion.

CHANGQING XU (Member, IEEE) received the B.S.E.E., M.S.E.E., and Ph.D.E.E. degrees from Shanghai Jiao Tong University, Shanghai, China, in 1989, 1993, and 2006, respectively. In 1994, he joined Shanghai Jiao Tong University, where he is currently a Professor with the Department of Electronic Engineering. His research interests include multiple-input multiple-output/orthogonal frequency-division multiplexing wireless systems, network coverage, routing, and node positioning algorithms in wireless sensor networks.